

ATTITUDE SENSING USING A GLOBAL-POSITIONING-SYSTEM ANTENNA ON A TURNTABLE

by Mark L. Psiaki*

Cornell University, Ithaca, N.Y. 14853-7501

Abstract

A new attitude sensor is proposed that consists of a single global positioning system (GPS) antenna mounted on a turntable with its phase center offset from the turntable's spin axis. It is being considered as a means of sensing 3-axis attitude information. It is attractive because its GPS receiver could have a low number of channels and, therefore, be smaller and use less power. The system senses attitude by demodulation of periodic oscillations of the GPS carrier phase. These oscillations are caused by the turntable's rotation, and their amplitude and phase depend on the direction vector to the tracked GPS satellite. This system is described in detail, its demodulation phase-locked loop is designed, and its performance is analyzed and evaluated via simulation. The computer simulation results show that, when using a turntable radius of 0.1 m, a rotation rate of 4,000 RPM, and an ovenized crystal oscillator for the receiver clock, the system can sense vector attitude with a 1- σ accuracy of 1.4 deg at a bandwidth of 0.64 Hz. Accuracy can be improved by increasing the turntable radius or by reducing multi-path reflections.

Introduction

Many different air, space, and marine vehicles need a 3-axis attitude determination system, and various types of sensor data can be used to determine the roll, pitch, and yaw orientations. The measured carrier phase of a Global Positioning System (GPS) signal is one such data type¹.

Attitude sensing based on GPS signals is attractive for several reasons. One is that a GPS receiver often is already part of a system because of its ability to sense position and velocity. If it can be made to sense attitude, then there will be a weight and power savings for the overall system because no additional attitude sensors will be needed. Alternatively, a GPS-based system can provide attitude determination redundancy. Yet a third attractive feature of GPS-based attitude sensing is the continuous availability of its signal. In low-Earth-orbit spacecraft applications, attitude data from sun sensors and from horizon sensors may not be

continuously available², but a well designed GPS-based system will not have this problem.

The standard GPS-based attitude sensing method uses multiple GPS antennas that are spatially distributed on the user vehicle. The receiver measures the carrier phase differences of the signal from a given GPS satellite. Each phase difference between an antenna pair gives the cosine of the angle between the vector to the GPS satellite and the vector from one antenna to the other. The former vector is known in inertial coordinates; the latter vector is known in vehicle body coordinates. Given enough of these cosine measurements, the full 3-axis attitude of the vehicle can be determined. The minimum number of receiver antennas is 3, and the minimum number of received GPS signals is 2¹.

There are several difficulties with the standard approach. One is the need to resolve phase ambiguities, which are integer cycle uncertainties in the carrier phase differences. Another problem is that the receiver may need to have many channels, one per antenna per satellite. A system that uses 4 antenna to track 6 GPS satellites might require 24 channels. This can require a high processor speed, which can increase the receiver's weight and power consumption. Yet a third problem with the traditional approach is that cosine-type attitude measurements are more difficult to use in a full 3-axis solution procedure than are vector-type measurements³.

Alternate schemes have been pursued for doing GPS-based attitude determination using fewer than 3 antennas⁴⁻⁶. The idea of Ref. 4 is to compute a pseudo-attitude based on the usual relationships between acceleration, velocity, and attitude for an aircraft. References 5 and 6 use two GPS antennas that are mounted on a spinning satellite. Their approach makes use of the known dynamics of a spinning, nutating spacecraft and deduces 3-axis attitude and attitude rate from the carrier phase differences between the signals that are received at the two antennas.

The present work presents a new way to use a single GPS antenna to sense 3 axis attitude information. A patch-type antenna is mounted on a spinning turntable. Its phase center is mounted off-axis, so that it translates around a circle as the turntable rotates. Its field of view is centered on the turntable's rotation axis so that its geometric gain pattern's inertial orientation does not vary significantly with table rotation. Figure

* Associate Professor, Sibley School of Mech. & Aero. Engr. Associate Fellow, AIAA.

Copyright Ó 2000 by Mark L. Psiaki. Published by the American Institute of Aeronautics and Astronautics, Inc., with permission.

1 is a schematic depiction of this system.

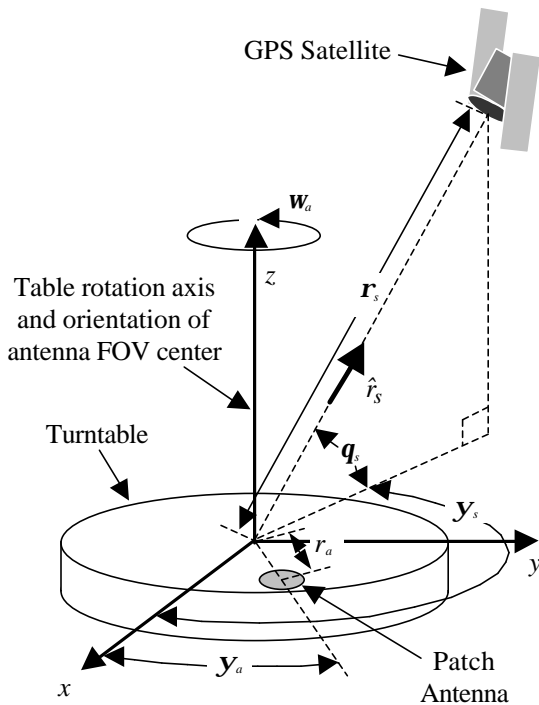


Fig. 1. Measurement geometry for attitude sensing based on a GPS antenna mounted on a turntable.

This system senses attitude by measuring a sinusoidal phase modulation of the GPS carrier signal. The circular motion of the antenna's phase center causes a received GPS signal's carrier phase to have a sinusoidally varying component because the motion creates sinusoidal variations of the distance from the antenna to the GPS satellite. This is effectively an FM-type component. The frequency of this modulation equals the rotation frequency of the table. The amplitude and phase of the modulation can be deduced by a specially designed phase-locked loop in the receiver. This amplitude and phase are uniquely related to the orientation, in table coordinates, of the vector to the GPS satellite. Therefore, this system provides vector-type attitude measurements. A similar concept has been used in the field of radio direction finding⁷.

This system is related to the 2-antenna systems of Refs. 5 and 6. Those systems and the present system each make use of circular motion of antenna phase centers in order to sense attitude. Attitude information is derived from time variations of GPS carrier phase signals.

There are some significant differences between the present system and those of Refs. 5 and 6. The present system does not rely on the spin of the vehicle to

create antenna motion. References 5 and 6 depend on having a good attitude dynamics model of the vehicle, but the present system does not need any such model so long as the attitude variations are not of too high a bandwidth. The systems of Refs. 5 and 6 use two antennas, but the present system uses only one. The present system can achieve a relatively high-bandwidth, on the order of 1 Hz. Attitude information is derived within the phase-locked loop that the receiver uses to track the GPS carrier signal. The systems of Ref. 5 and 6, on the other hand, have very low bandwidths – Ref. 6 requires data batches of 50 to 400 sec in duration in order to deduce attitude.

This new system has been considered because it has several important advantages. First, it can provide enough data to determine 3-axis attitude by tracking only 2 GPS satellites, which requires only 2 receiver channels. Second, this system does not require resolution of integer phase cycle ambiguities because attitude is sensed from the time history of the carrier phase of a single antenna, not from phase differences between multiple antenna. Third, this system can be built mostly out of existing hardware. The necessary hardware includes a receiver whose phase-locked loops can be re-programmed and turntables of appropriate diameter and speed. In fact, there exist open-architecture GPS receivers whose tracking loops can be re-programmed⁸, and there exist suitable turntables, ones which are already being used on spacecraft to provide attitude sensing while simultaneously augmenting the pitch-axis angular momentum⁹.

This paper's 5 main sections accomplish its goals of defining, explaining, and evaluating this new system. Section 2 defines the system's hardware configuration. Section 3 explains what its measurements are and how these are related to attitude. Section 4 designs and analyzes a phase-locked loop that is used to demodulate the attitude information. Section 5 describes a simulation that has been used to evaluate the system's performance. Simulation results are presented in Section 6 along with analysis results. The paper closes with a short conclusions section that summarizes its contributions.

II. Description of System Hardware Components

This section describes the basic hardware requirements for the design of the system that is depicted schematically in Fig. 1. As stated above, the system needs a turntable, a GPS antenna mounted on the turntable, and a receiver that is connected to that antenna. In addition, the turntable needs to have a speed controller, and it needs to have an encoder so that the turntable's rotational phase, y_a on Fig. 1, is

always available to the receiver.

The turntable is envisioned as being like a typical spacecraft scan wheel that is used for simultaneous pitch axis momentum augmentation and horizon sensing⁹. Its diameter would be on the order of 0.25 m, and it would be able to rotate at speeds up to 4,000 RPM. Slower turntable speeds are acceptable, and larger turntable diameters will tend to increase the system's accuracy, but these numbers have been used as baselines because they are typical of hardware that is currently used on a number of spacecraft. The accuracy of the turntable's position encoder is important. The receiver needs to know $\mathbf{y}_a(t)$ in order to deduce the azimuth of the direction vector to each tracked GPS satellite, \mathbf{y}_s . Any error in \mathbf{y}_a will translate directly into an error in \mathbf{y}_s . Therefore, the required encoder accuracy is 0.1 deg or better.

The antenna should be a patch-type antenna. These can be made with a diameter on the order of 0.05 m. This allows the phase center to be mounted at a significant distance from the turntable rotation axis. The nominal mounting radius assumed for this study is $r_a = 0.1$ m.

The antenna field of view must be fairly wide, and its center must be aligned with the turntable's rotation axis. The idea is to have a wide enough field of view so that the system can always see at least 2 GPS satellites.

System geometry is important in order to get good signal reception. The turntable needs to be cantilevered on its bearings so that the antenna has a clear view of the sky during the whole rotation cycle. The turntable should have a ground plane for the antenna; i.e., its outer face should be a ground plane. Also, the turntable/antenna system should be mounted on the user vehicle in a place that minimizes multi-path interference. It may be a good idea to restrict the antenna field of view somewhat if that will help to reduce multi-path signal reception.

The receiver can be a standard receiver as in Ref. 8. There are three important features that the receiver must have. First, it must be able to accept turntable azimuth readings from the turntable encoder and synchronize them with its correlator accumulations. Second, it must have a special purpose phase-locked loop that measures the in-phase and quadrature components of the turntable-synchronous carrier phase oscillation. Any open-architecture receiver should be modifiable to have the requisite phase-locked loop. Third, if one wants to do 3-axis attitude determination, then the receiver must have at least 2 channels so that it can simultaneously track at least 2 GPS satellites.

The final requirement of the hardware design is that it must transmit the 1575.42 MHz L₁ signal from the

antenna to the receiver's radio-frequency (RF) front end without significant loss of signal-to-noise ratio (SNR). In order to do this, one must transmit the RF signal across a rotary joint, or one must mount the receiver on the turntable. In the latter case, the system will have to transmit power to the receiver across the rotary joint, and the receiver's attitude estimate will have to get transmitted back across the rotary joint. If the receiver is not mounted on the turntable, then a rotary capacitive coupling can be used to transmit the RF signal across the rotary joint.

III. Measurement Model

The geometry of Fig. 1 can be used to explain why this system's measurements give attitude. Assume that the rotating turntable in the figure is mounted on a user vehicle and that the user vehicle's attitude varies slowly compared to the rotation speed of the turntable. The following are the significant geometric and kinematic features of the system: The xyz coordinate-system is fixed to the user vehicle. It does not rotate with the turntable, but its z axis is aligned with the turntable's rotation axis, and its x - y plane is the plane in which the patch antenna's phase center moves. The patch antenna's location in the xyz coordinate system is defined by the rotation angle \mathbf{y}_a and the radial offset r_a . The turntable rotates at a constant speed \mathbf{w}_a . Therefore, $\mathbf{y}_a(t) = \mathbf{w}_a t + \mathbf{y}_{a0}$. The GPS satellite's position in the xyz coordinate system is defined by its azimuth, \mathbf{y}_s , elevation, \mathbf{q}_s , and distance from the origin, \mathbf{r}_s . Typically, r_a will be on the order of 0.1 m, while \mathbf{r}_s will be on the order of 26×10^6 m. Therefore, $(r_a/\mathbf{r}_s) \ll 1$.

The user vehicle attitude can be determined if the receiver can sense \mathbf{y}_s and \mathbf{q}_s for two or more GPS spacecraft that are not collinear with the user vehicle. The quantities \mathbf{y}_s and \mathbf{q}_s define the direction to the GPS spacecraft, $\hat{\mathbf{r}}_s$, in user vehicle coordinates. Given knowledge of the user vehicle location, this same vector is known in inertial coordinates. It is well known that one can uniquely deduce 3-axis attitude given knowledge of two or more independent direction vectors both in vehicle coordinates and in inertial coordinates¹⁰. This is why the proposed system can be used to determine the full 3-axis attitude if it can track 2 or more GPS satellites.

In order to understand how to deduce \mathbf{y}_s and \mathbf{q}_s from carrier phase measurements, consider the range from the user antenna to the GPS satellite. From geometry, the range between the antenna and the satellite is:

$$\begin{aligned} r_{as} &= \sqrt{\mathbf{r}_s^2 + r_a^2 - 2\mathbf{r}_s r_a \cos \mathbf{q}_s \cos(\mathbf{w}_a t + \mathbf{y}_{a0} - \mathbf{y}_s)} \\ &\cong \mathbf{r}_s - r_a \cos \mathbf{q}_s \cos(\mathbf{w}_a t + \mathbf{y}_{a0} - \mathbf{y}_s) \end{aligned} \quad (1)$$

where the approximation on the second line of eq. (1)

is valid for $(r_a/r_s) \ll 1$.

The range to the GPS satellite can be used to deduce an expression for the received carrier phase. If w_c is the transmission frequency of the signal in radians/sec, then

$$\begin{aligned} \mathbf{f}_c(t) &= \mathbf{w}_c t - \mathbf{r}_{as}(t) \left(\frac{w_c}{c} \right) + \text{constant} \\ &= \mathbf{w}_c t + \mathbf{f}_{Dopp}(t) \end{aligned} \quad (2)$$

where \mathbf{f}_c is the received carrier phase in radians and c is the speed of light. The term $\mathbf{f}_{Dopp}(t)$ is the integrated effect on the carrier phase of the signal's Doppler shift. An alternate expression for the received carrier phase can be derived by substituting the 2nd line of eq. (1) into eq. (2):

$$\begin{aligned} \mathbf{f}_c(t) &= \mathbf{w}_c t + \mathbf{f}_{Dmr}(t) + x_c \cos(\mathbf{w}_a t + \mathbf{y}_{a0}) \\ &\quad + x_s \sin(\mathbf{w}_a t + \mathbf{y}_{a0}) \end{aligned} \quad (3)$$

The term $\mathbf{f}_{Dmr}(t)$ is the Doppler-induced phase perturbation that would be present if there were no turntable rotation. This quantity constitutes what is usually known as the integrated Doppler shift or the accumulated delta range¹¹. The last two terms on the right-hand side of eq. (3) give the effects on carrier phase of the turntable's rotation. The coefficients x_c and x_s are

$$x_c = \frac{w_c r_a}{c} [\cos \mathbf{q}_s \cos \mathbf{y}_s] \quad (4a)$$

$$x_s = \frac{w_c r_a}{c} [\cos \mathbf{q}_s \sin \mathbf{y}_s] \quad (4b)$$

The quantities \mathbf{y}_s and \mathbf{q}_s can be deduced from eqs. (4a) and (4b). Suppose that r_a is known and that x_c and x_s have been measured by the receiver – Section 4 of this paper will show how to do this. Then the only unknowns in eqs. (4a) and (4b) are \mathbf{y}_s and \mathbf{q}_s , and these equations can be inverted to yield the formulas

$$\mathbf{y}_s = \arctan 2(x_s, x_c) \quad (5a)$$

$$\mathbf{q}_s = \arccos[(c\sqrt{x_c^2 + x_s^2})/(w_c r_a)] \quad (5b)$$

IV. A Phase-Locked Loop for Tracking Sinusoidal Carrier Phase Variations

A coherent GPS receiver uses a phase-locked loop to reconstruct the carrier phase inside of the receiver. Figure 2 shows a high-level block diagram of a typical channel of a coherent GPS receiver^{12,13}. The RF front end starts with the signal from the antenna and pre-amp, $y_{rf}(t)$, and performs band-pass filtering and down-conversion via mixing. Its output signal, $y_{if}(t)$, has a nominal intermediate frequency (IF) of w_{if} . The carrier phase numerically controlled oscillator (NCO) constructs in-phase and quadrature approximations of the down-converted carrier signal, $\cos[\mathbf{w}_{if} t + \mathbf{f}_{re}(t)]$ and $-\sin[\mathbf{w}_{if} t + \mathbf{f}_{re}(t)]$. These signals are mixed with $y_{if}(t)$

to form the base-band in-phase and quadrature signals, $y_i(t)$ and $y_q(t)$. The delay-locked loop (DLL) correlates these signals with a reconstruction of the pseudo-random (PRN) code of the GPS satellite that is being tracked, and it adjusts its play-back rate of the PRN code so as to maximize the correlation. In the process, the DLL produces in-phase and quadrature accumulations, I_n and Q_n , once every PRN code period, i.e., about once every 0.001 sec. The loop filter of the phase-locked loop (PLL) uses the I_n and Q_n accumulations to adjust the frequency of the carrier phase NCO by adjusting w_{re} ($= d\mathbf{f}_{re}/dt$). This quantity is nominally the PLL's estimate of the carrier signal's Doppler shift because $\mathbf{f}_{re}(t)$ is nominally the PLL's estimate of $\mathbf{f}_{Dopp}(t)$.

In the present system, the PLL's loop filter is constructed to estimate x_c and x_s as part of the procedure by which it computes w_{re} . Recall from eq. (3) that x_c and x_s are the coefficients of the two components of the carrier phase that oscillate at the turntable frequency. The PLL estimates x_c and x_s as part of a Kalman filter. In order to develop this Kalman filter, it is necessary to develop a stochastic model that describes the dynamics of $\mathbf{f}_{Dopp}(t)$ and the effect of $\mathbf{f}_{Dopp}(t)$ on the measurements I_n and Q_n .

Carrier Phase Model

A discrete-time carrier phase model has been developed. Suppose that the DLL's PRN code cycles start and end at the sample times $t_0, t_1, t_2, \dots, t_n, \dots$. Then the carrier phase dynamic model is

$$\begin{aligned} \begin{bmatrix} x_p \\ x_v \\ x_a \\ x_c \\ x_s \end{bmatrix}_n &= \begin{bmatrix} 1 & \mathbf{D}t_{n-1} & \frac{\mathbf{D}t_{n-1}^2}{2} & 0 & 0 \\ 0 & 1 & \mathbf{D}t_{n-1} & 0 & 0 \\ 0 & 0 & 1 & 0 & 0 \\ 0 & 0 & 0 & 1 & 0 \\ 0 & 0 & 0 & 0 & 1 \end{bmatrix} \begin{bmatrix} x_p \\ x_v \\ x_a \\ x_c \\ x_s \end{bmatrix}_{n-1} \\ &- \begin{bmatrix} \mathbf{D}t_{n-1} \\ 0 \\ 0 \\ 0 \\ 0 \end{bmatrix} \mathbf{w}_{re(n-1)} + \begin{bmatrix} \frac{\mathbf{D}t_{n-1}^2}{6} & 0 & 0 \\ \frac{\mathbf{D}t_{n-1}}{2} & 0 & 0 \\ 1 & 0 & 0 \\ 0 & 1 & 0 \\ 0 & 0 & 1 \end{bmatrix} \mathbf{w}_{n-1} \end{aligned} \quad (6a)$$

$$\begin{aligned} \mathbf{f}_{Dopp}(t_n) &= \mathbf{f}_{re}(t_n) + x_{p(n)} + x_{c(n)} \cos(\mathbf{w}_a t_n + \mathbf{y}_{a0}) \\ &\quad + x_{s(n)} \sin(\mathbf{w}_a t_n + \mathbf{y}_{a0}) \end{aligned} \quad (6b)$$

In this model $\mathbf{D}t_{n-1} = t_n - t_{n-1}$. The frequency $w_{re(n-1)}$ is the value of $d\mathbf{f}_{re}/dt$ during the time interval t_{n-1} to t_n . The state $x_p = \mathbf{f}_{Dmr} - \mathbf{f}_{re} + \mathbf{w}_a t$, the integrated Doppler shift due to translation of the center of the turntable relative to the GPS satellite minus the carrier NCO's

approximate integrated Doppler shift plus a term that arises due to carrier phase wrap-up. Wrap-up is a combined effect of the signal's polarization and the antenna's attitude rotation about its field-of-view centerline. The state $x_v = \dot{\mathbf{f}}_{Dnr} + \mathbf{w}_s$, the Doppler shift due to the velocity of the turntable center relative to the GPS satellite plus another carrier phase wrap-up term. The state $x_a = \ddot{\mathbf{f}}_{Dnr}$, the rate of change of Doppler shift due to the acceleration of the turntable center relative to the GPS satellite.

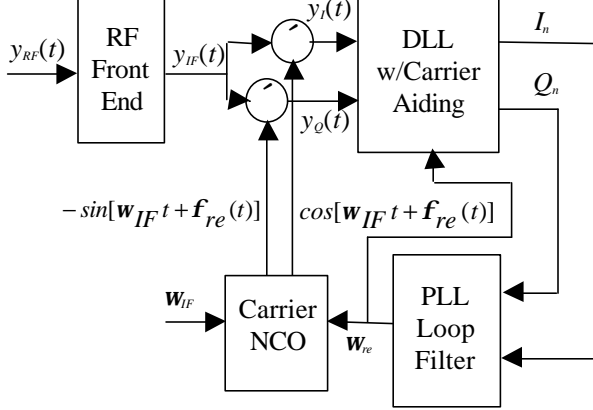


Fig. 2. Block diagram of a single channel of a coherent GPS receiver.

The 3×1 vector w_{n-1} in eq. (6a) is the discrete-time white noise process disturbance. It models the effects of receiver vehicle maneuvers. It has the following statistical model:

$$E\{w_{n-1}\} = 0 \quad (7a)$$

$$E\{w_{m-1}w_{n-1}^T\} = \mathbf{d}_{mn} \mathbf{D}t_{n-1} \begin{bmatrix} q_a & 0 & 0 \\ 0 & q_{cs} & 0 \\ 0 & 0 & q_{cs} \end{bmatrix} \quad (7b)$$

where \mathbf{d}_{mn} is the Kronecker delta and q_a and q_{cs} are equivalent continuous-time white noise intensities. The modeled values of q_a and q_{cs} can be used to tune the resulting Kalman filter.

The model in eqs. (6a) and (6b) allows Kalman filter estimation of both the attitude parameters x_c and x_s and the velocity and acceleration of the line-of-sight from the center of the turntable to the tracked GPS satellite. The ability to deal with non-zero velocity and acceleration is obviously important for vehicles. The ability is also important for static receivers because the motion of the GPS satellite causes significant relative velocity and acceleration.

The measurement that is used in the Kalman filter is derived from the DLL's in-phase and quadrature accumulations. It is a carrier phase error measurement:

$$y_n = -\arctan2(Q_n, I_n) \quad (8)$$

If the receiver has achieved lock on the signal, then this measurement can be modeled as the average difference between the NCO's phase and the actual carrier phase. The average is taken over the time interval from t_{n-1} to t_n :

$$y_n = \frac{1}{\mathbf{D}t_{n-1}} \int_{t_{n-1}}^{t_n} [x_p(t) + x_c(t) \cos(\mathbf{w}_a t + \mathbf{y}_{a0}) + x_s(t) \sin(\mathbf{w}_a t + \mathbf{y}_{a0})] dt + v_n \quad (9)$$

where v_n is a Gaussian random measurement error that is caused by thermal noise and digitization. Its mean is zero, its variance is \mathbf{s}_v^2 , and it is uncorrelated in time and uncorrelated with w_{n-1} .

This measurement can be modeled in terms of the state vector of eq. (6a). The following measurement equation has been derived by substitution into eq. (9) of the underlying continuous-time model that has been used to derive eq. (6a):

$$y_n = \begin{bmatrix} 1 & \frac{\mathbf{D}t_{n-1}}{2} & \frac{\mathbf{D}t_{n-1}^2}{6} & C_{c(n-1)} & C_{s(n-1)} \end{bmatrix} \begin{bmatrix} x_p \\ x_v \\ x_a \\ x_c \\ x_s \end{bmatrix}_{n-1} - \frac{\mathbf{D}t_{n-1}}{2} \mathbf{w}_{re(n-1)} + \begin{bmatrix} \frac{\mathbf{D}t_{n-1}^2}{24} & D_{c(n-1)} & D_{s(n-1)} \end{bmatrix} w_{(n-1)} + v_n \quad (10)$$

The coefficients in eq. (10) are

$$C_{c(n-1)} = \left[\frac{\sin(\mathbf{w}_a t_n + \mathbf{y}_{a0}) - \sin(\mathbf{w}_a t_{n-1} + \mathbf{y}_{a0})}{\mathbf{w}_a \mathbf{D}t_{n-1}} \right] \quad (11a)$$

$$C_{s(n-1)} = - \left[\frac{\cos(\mathbf{w}_a t_n + \mathbf{y}_{a0}) - \cos(\mathbf{w}_a t_{n-1} + \mathbf{y}_{a0})}{\mathbf{w}_a \mathbf{D}t_{n-1}} \right] \quad (11b)$$

$$D_{c(n-1)} = - \left[\frac{C_{s(n-1)} - \sin(\mathbf{w}_a t_n + \mathbf{y}_{a0})}{\mathbf{w}_a \mathbf{D}t_{n-1}} \right] \quad (11c)$$

$$D_{s(n-1)} = \left[\frac{C_{c(n-1)} - \cos(\mathbf{w}_a t_n + \mathbf{y}_{a0})}{\mathbf{w}_a \mathbf{D}t_{n-1}} \right] \quad (11d)$$

The discrete-time model in eqs. (6a) and (10) takes the following form:

$$x_n = \mathbf{F}_{n-1} x_{n-1} + \mathbf{G}_{n-1} w_{re(n-1)} + \mathbf{G}_{w(n-1)} w_{n-1} \quad (12a)$$

$$y_n = C_{n-1} x_{n-1} + D_{n-1} w_{re(n-1)} + D_{w(n-1)} w_{n-1} + v_n \quad (12b)$$

The 5×1 state vector in this model is $x = [x_p, x_v, x_a, x_c, x_s]^T$. The matrices \mathbf{F}_{n-1} , \mathbf{G}_{n-1} , and $\mathbf{G}_{w(n-1)}$ are effectively defined by eq. (6a), and the matrices C_{n-1} , D_{n-1} , and $D_{w(n-1)}$ are defined by eq. (10).

This time-varying system's 5×5 observability Gramian matrix has been calculated for one turntable rotation period. It has a rank of 5, which proves the system's observability¹⁴. Therefore, the system states can be estimated from the carrier phase error measurements.

Kalman Filter to Estimate Carrier Phase States

A Kalman filter can be used to estimate the states of the phase model in eqs. (12a) and (12b). The Kalman filter keeps track of the estimated state vector, \hat{x} . It can be implemented via the following combined propagation and update equations:

$$\bar{v}_n = y_n - [C_{n-1} \hat{x}_{n-1} + D_{n-1} \mathbf{w}_{re(n-1)}] \quad (13a)$$

$$\hat{x}_n = \mathbf{F}_{n-1} \hat{x}_{n-1} + \mathbf{G}_{n-1} \mathbf{w}_{re(n-1)} + L_n \bar{v}_n \quad (13b)$$

In these equations the scalar \bar{v}_n is the filter innovation, and L_n is the 5×1 filter gain matrix.

The filter gain matrix will be time-varying due to the time variations in the system model. The most important time variations are the sinusoidal variations of $C_{c(n-1)}$ and $C_{s(n-1)}$, which are elements of the C_{n-1} matrix. Normally L_n would be computed using a time propagation of a matrix Riccati equation, which, in this case, would have to be specially designed to account for the appearance of the process noise w_{n-1} in the measurement equation¹⁴. If the turntable's rotation rate ω_a is very slow or if the Kalman filter needs to have a high bandwidth, then this way of computing L_n will definitely be needed.

In the present case it is sometimes possible to compute a time varying filter gain without propagating a matrix Riccati equation. The following filter gain is approximately optimal when the Kalman filter's bandwidth is lower than the turntable rotation speed:

$$L_n = \begin{bmatrix} L_{pva} \\ L_{cs} C_{c(n-1)} \\ L_{cs} C_{s(n-1)} \end{bmatrix} \quad (14)$$

The quantity L_{pva} is a constant 3×1 steady-state gain matrix. It can be derived by solving a steady-state, time-invariant Kalman filter problem. This problem is for a modified form of eqs. (6a) and (10), one that deletes the states x_c and x_s and the 2nd and 3rd elements of the process noise disturbance vector w . Also, D_{n-1} is set equal to its nominal value of 0.001 sec.

The scalar gain L_{cs} can be determined by an averaging technique that solves a time-invariant Kalman filter problem for an average of the system over one period of the turntable's rotation, $2\mathbf{p}/\omega_a$. Such techniques have been found to work well for periodic systems whose closed-loop bandwidth is low compared to the frequency of periodicity¹⁵. Note that, in the case of a Kalman filter, loop closure refers to

the feeding back of the innovation to correct the state estimate, as in eq. (13b). L_{cs} is the scalar gain that would be used in the eq.-(13b) form of the steady-state Kalman filter for the following scalar, time-invariant problem:

$$x_{cs(n)} = x_{cs(n-1)} + w_{cs(n-1)} \quad (15a)$$

$$y_{cs(n)} = 0.5x_{cs(n-1)} + 0.25w_{cs(n-1)} + v_{cs(n)}/\sqrt{2} \quad (15b)$$

where $E\{w_{cs(n-1)}\} = 0$, $E\{w_{cs(m-1)}w_{cs(n-1)}\} = \mathbf{d}_{mm} q_{cs}$ (0.001 sec), $E\{v_{cs(n)}\} = 0$, $E\{v_{cs(m)}v_{cs(n)}\} = \mathbf{d}_{mm} \mathbf{s}_v^2$, and $E\{w_{cs(m-1)}v_{cs(n)}\} = 0$. In this model $w_{cs(n-1)}$ is equivalent to the 2nd element of w_{n-1} in eq. (6a) and $v_{cs(n)}$ is equivalent to v_n in eq. (10). Equation (15a) is equivalent to the fourth line of eq. (6a), and eq. (15b) is equivalent to eq. (10) multiplied by $C_{c(n-1)}$ and averaged over a turntable rotation period. Alternatively, $w_{cs(n-1)}$ is equivalent to the 3rd element of w_{n-1} in eq. (6a), and eqs. (15a) and (15b) can be derived by using the fifth line of eq. (6a) and by multiplying eq. (10) by $C_{s(n-1)}$ and averaging over a turntable period. This technique works because the filter's error dynamics converge slowly compared to the turntable rotation period and because $\text{average}(C_{c(n-1)}^2) = \text{average}(C_{s(n-1)}^2) = 0.5$ while $\text{average}(C_{c(n-1)}) = \text{average}(C_{s(n-1)}) = \text{average}(C_{c(n-1)}C_{s(n-1)}) = 0$. These facts combine to yield filters for the three state components $[x_p, x_v, x_a]^T$, x_c , and x_s that are approximately decoupled, and the composite gain for these three filters is well approximated by the form given in eq. (14).

Use of the Kalman Filter Output to Drive the Carrier NCO

The phase locked loop needs to feed back y , the phase error, to \mathbf{w}_{re} , the frequency of the carrier tracking NCO. The Kalman filter, although it gives optimal estimates of the components of the phase error, gives no guidance on how to pick \mathbf{w}_{re} . In theory, the filter can function properly with an arbitrary \mathbf{w}_{re} . In practice, it is necessary to choose \mathbf{w}_{re} so as to stabilize y to a value near zero. Otherwise, cycle slips can occur due to the $2\mathbf{p}$ indeterminacy of eq. (8), or the assumptions of this whole analysis can break down due to poor PRN code correlation when the carrier NCO frequency is far different from the incoming signal's intermediate frequency.

The phase-locked loop's feedback control law uses the states of the Kalman filter to determine \mathbf{w}_{re} . The PLL assumes that $\mathbf{w}_{re(n)}$ has already been chosen by the time the Kalman filter's estimate \hat{x}_n is available. Therefore, it uses \hat{x}_n to determine $\mathbf{w}_{re(n+1)}$ according the following rule: the predicted value of the phase error at time t_{n+2} must equal \mathbf{a} times the estimated phase error at time t_n , where \mathbf{a} is an arbitrary tuning factor for the

PLL that is in the range $0 \leq \mathbf{a} < 1$. This rule is embodied in the following formula for the NCO frequency:

$$\begin{aligned} \mathbf{w}_{re(n+1)} = & \{-\mathbf{D}t_n \mathbf{w}_{re(n)} + (I-\mathbf{a}) \hat{x}_{p(n)} \\ & + (\mathbf{D}t_n + \mathbf{D}t_{n+1}) \hat{x}_{v(n)} + 0.5(\mathbf{D}t_n + \mathbf{D}t_{n+1})^2 \hat{x}_{a(n)} \\ & + [\cos(\mathbf{w}_a t_{n+2} + \mathbf{y}_{a0}) - \mathbf{a} \cos(\mathbf{w}_a t_n + \mathbf{y}_{a0})] \hat{x}_{c(n)} \\ & + [\sin(\mathbf{w}_a t_{n+2} + \mathbf{y}_{a0}) - \mathbf{a} \sin(\mathbf{w}_a t_n + \mathbf{y}_{a0})] \hat{x}_{s(n)} \} / \mathbf{D}t_{n+1} \end{aligned} \quad (16)$$

The Kalman filter and this \mathbf{w}_e feedback law constitute the PLL loop filter that is shown in Fig. 2. The equations that get implemented in this digital filter are eqs. (8), (13a), (13b), and (16). Equation (8) can be implemented efficiently and without significant loss of SNR by using an approximation to the 2-argument arctangent function.

PLL Tuning

The feedback control law in eq. (16) will cause the PLL to converge to zero phase error with a first-order response. The time constant of this decay will be $t_{pll} = -2(0.001 \text{ sec})/\ln(\mathbf{a})$. The performance of the Kalman filter is theoretically independent of the actual value of this time constant. t_{pll} should be chosen small enough to keep the phase errors from becoming too large, but not too small, otherwise system noise will cause excessive jitter of the carrier NCO frequency. A value of $\mathbf{a} = 0.8$ has been used throughout most of this study, which translates into a settling time constant of $t_{pll} = 9 \text{ msec}$.

The overall bandwidth of the PLL is governed by t_{pll} and by the error decay time constants of the Kalman filter. These latter time constants are determined by the Kalman filter gain parameters L_{pva} and L_{cs} . When t_{pll} is small, the effective bandwidth of the PLL is governed primarily by the values of the Kalman filter gains.

Dealing with GPS Data Bits

An actual system must be able to deal with phase shifts that occur due to the transmission of data bits. In a real GPS system, data bits are encoded on the signal at a rate of 50 bits/sec. This introduces the possibility of 180 deg phase shifts of \mathbf{f}_{Dopp} once every 20 PRN code periods. Extra logic is needed in a real receiver to avoid the possibility that the PLL will interpret such a phase shift as a change of \mathbf{f}_{Dopp} due to an actual Doppler shift. The necessary logic is not hard to implement if the receiver is already tracking a signal that has a large SNR. The problem becomes trickier when one is trying to achieve phase lock on a signal that has a low SNR. The problem of data bit logic is not addressed in the present paper.

V. Simulation of the GPS Signal and the Rotating Antenna/Receiver System

A simulation of this system has been developed. It is for use in evaluating the system's functioning and accuracy. The simulation includes the following components: the PRN-code-modulated signals of the tracked GPS satellite and of interfering satellites, the thermal and digitization noise of the receiver, the receiver clock drift, the down-converting mixers and band-pass filters of the RF front end, the carrier NCO, mixers, and loop filter of the PLL, and the PRN code NCO, correlators, and loop filter of the DLL. The simulation implements time-domain models of the system's major elements.

Thermal and digitization noise typically arise from different elements within a circuit, but the simulation lumps all of the noise at the receiver input and characterizes it by an equivalent total input noise temperature. The receiver noise temperature in the simulation has been sized to match what has been observed experimentally in a terrestrial application. This experiment used a typical receiver⁸, a patch antenna with a hemispherical gain pattern, and a low-noise preamplifier. The system's front end had a gain of 31 dB and a noise figure of 2.5 dB as measured from the antenna input to the receiver input.

Most of the RF signals in the simulation are represented by their complex envelopes. A complex envelop representation takes the form:

$$y_z(t) = \text{real}\{s_z(t)e^{j\mathbf{w}t}\} \quad (17)$$

where $y_z(t)$ is a band-limited signal in a frequency band centered at the carrier frequency \mathbf{w} , $s_z(t)$ is the base-band complex envelop of $y_z(t)$, and $j = \sqrt{-1}$. It can be shown that any band-limited signal can be represented in this way, and it is straightforward to model the effects of mixers and band-pass filters on a signal's complex envelop representation¹⁶.

GPS Signal Model. The simulation starts by constructing a complex envelop representation of the incoming GPS signal. Each GPS satellite signal consists of a sine wave that is Doppler shifted from the nominal 1575.42 MHz L_1 carrier frequency and that has its pseudo-random code modulated onto it via binary phase-shift keying. Suppose that the incoming signal is $y_{RF}(t)$ and that its complex envelop is $s_{RF}(t)$, similar to eq. (17). Then the center frequency is $\mathbf{w} = \mathbf{w}_e = 2\mathbf{p} \times 1575.42 \times 10^6 \text{ rad/sec}$, and the complex envelop is

$$s_{RF}(t) = \sum_{i=1}^N \left\{ A^i C^i [t^i(t)] \exp[j\mathbf{f}_{Dopp}^i(t)] \right\} + v_{RF}(t) \quad (18)$$

The i superscript in this equation refers to GPS

satellite i . The amplitude A^i sets the signal power. The function $C^i(\mathbf{t})$ is the satellite's ± 1 pseudo-random code, and $\mathbf{t}^i(t)$ is the pseudo-random code phase measured in code seconds. The PRN code repeats itself with a period of $D\mathbf{t} = 0.001$ code sec. The quantity $\mathbf{f}_{Dopp}^i(t)$ is the integrated Doppler shift of the carrier signal. Note that $\mathbf{t}^i(t) = t + [\mathbf{f}_{Dopp}^i(t)/\mathbf{w}_c] + \text{constant}$. The signal $v_{RF}(t)$ is a complex envelop representation of the equivalent total thermal and digitization noise of the antenna plus the receiver. The simulation only attempts to track one of the GPS satellite signals. The others are included to simulate multi-channel interference.

Each $\mathbf{f}_{Dopp}^i(t)$ time history is determined from the GPS satellite range time history and the table rotation time history according to the following formulas, which are consistent with eqs. (1) and (2):

$$\mathbf{f}_{Dopp}^i(t) = \text{constant} - (\mathbf{w}_c/c) \bullet \sqrt{[\mathbf{r}_s^i(t)]^2 + r_a^2 - 2\mathbf{r}_s^i(t)r_a \cos \mathbf{q}_s^i \cos(\mathbf{w}_a t + \mathbf{y}_{a0} - \mathbf{y}_s^i)} \quad (19)$$

where

$$\mathbf{r}_s^i(t) = \mathbf{r}_{s0}^i + \dot{\mathbf{r}}_{s0}^i t + 0.5 \ddot{\mathbf{r}}_s^i t^2 \quad (20)$$

\mathbf{r}_{s0}^i is the initial distance from the turntable center to GPS satellite i , $\dot{\mathbf{r}}_{s0}^i$ is the initial range rate, and $\ddot{\mathbf{r}}_s^i$ is the range acceleration.

The simulation assumes that each GPS satellite has a nonzero initial line-of-sight velocity, $\dot{\mathbf{r}}_{s0}^i$, and a nonzero line-of-sight acceleration, $\ddot{\mathbf{r}}_s^i$. The initial line-of-sight rates have been chosen randomly to fall in the range $\pm 8,600$ m/sec, which is consistent with the possible range of relative velocities for a user satellite in low Earth orbit. The line-of-sight accelerations have been chosen randomly to fall in the range ± 5 g's. Although this large range for the accelerations is probably excessive, it serves to make the point that large accelerations do not adversely affect the system's performance.

The simulation uses the actual GPS C/A pseudo-random codes. They are generated by computer code that emulates simple feedback shift registers¹⁷.

The simulation uses a sampled version of the signal. If the sample interval is defined to be $D\mathbf{t}_{sim}$, then the sampled signal is

$$\begin{aligned} s_{RF(m)} &= s_{RF}(mD\mathbf{t}_{sim}) \\ &= \sum_{i=1}^N \left\{ A^i C^i[\mathbf{t}^i(mD\mathbf{t}_{sim})] \exp[j\mathbf{f}_{Dopp}^i(mD\mathbf{t}_{sim})] \right\} \end{aligned}$$

$$+ v_{RF(m)} \quad (21)$$

where m is the sample index and $v_{RF(m)}$ is a sampled-data version of the RF noise model.

The nominal sample period that has been used is $D\mathbf{t}_{sim} = 81.46$ nanosec. This yields 12 samples per pseudo-random code chip, which is adequate to represent the digital code signals $C^i(\mathbf{t})$. The sampling frequency is $1/D\mathbf{t}_{sim} = 12.3$ MHz. This is significantly more than twice the 1 MHz bandwidth of the intermediate RF signal that comes out of each receiver's RF front end, $y_{IF}(t)$, which implies that this sample period is adequately small.

The thermal/digitization noise model is represented by the discrete-time Gaussian white-noise sequence $v_{RF(0)}, v_{RF(1)}, v_{RF(2)}, \dots, v_{RF(m)}, \dots$. Its standard deviation is

$$\mathbf{s}_{noise} = \sqrt{kT_{rcvr} / D\mathbf{t}_{sim}} \quad (22)$$

where k is Boltzmann's constant and T_{rcvr} is the equivalent input noise temperature of the receiver in degrees Kelvin. The discrete-time noise sequence is then

$$\mathbf{n}_m = \mathbf{s}_{noise} [\mathbf{n}_{real(m)} + j\mathbf{n}_{imag(m)}] \quad (23)$$

In this model $\mathbf{n}_{real(m)}$ and $\mathbf{n}_{imag(m)}$ are both real, zero-mean, unit-variance, uncorrelated discrete-time white-noise processes, which are simulated by a random number generator.

One significant error source has been neglected in this simulation model, multi-path noise. It has been neglected because it is too difficult to model. It is best studied via experiment. For completeness sake, however, a later section of this paper estimates the magnitude of multi-path-induced attitude measurement errors.

Complex Envelop Simulation of the Receiver's RF Front End. The RF front end of the receiver is modeled by 3 stages of band-pass filtering that alternate with two stages of mixing. It produces a signal $y_{IF}(t)$ whose intermediate frequency is nominally 3.636 MHz and whose bandwidth is approximately 1 MHz. The mixers and filters are modeled by appropriate band-pass modeling techniques¹⁶. The last band-pass filter model, the one with a 1 MHz bandwidth, has a 5-pole complex envelop representation. Its 5 poles fall in an asymmetrical Butterworth-like pattern. Its model matches experimental frequency response data from an actual filter.

PLL and DLL Simulation. This section describes the simulation of everything that is downstream of the RF front-end: the in-phase and quadrature mixers, the DLL, the PLL's loop filter, and the carrier NCO. The input to this part of the simulation is $y_{IF}(t)$, the intermediate frequency signal that comes out of the

receiver's RF front end – review Fig. 2.

This part of the simulation bases its calculations on time intervals, each of which corresponds to the receiver's estimate of a distinct period of the PRN code of the tracked satellite. The boundaries of these time intervals are $t_0, t_1, t_2, \dots, t_n, \dots$. At these sample times the receiver's estimated code phase is always an integer multiple of the nominal code period of 0.001 sec.; i.e., $\hat{\mathbf{f}}(t_n) = n \times 0.001$, where $\hat{\mathbf{f}}(t)$ is the DLL's estimated code phase at time t .

This part of the simulation works entirely with real signals. Before mixing the signal to base-band, it uses the complex envelop $s_{IF}(t)$ to compute the actual signal that comes out of the RF front-end: $y_{IF}(t) = \text{real}\{s_{IF}(t)e^{j\mathbf{w}_{IF}t}\}$.

The next operation is the generation of the outputs of the in-phase and quadrature carrier mixers. They are

$$y_I(t) = \cos[\mathbf{w}_{IF}t + \mathbf{w}_{re(n-1)}(t-t_{n-1}) + \hat{\mathbf{f}}_{re(n-1)}]y_{IF}(t) \quad \text{for } t_{n-1} \leq t < t_n \quad (24a)$$

$$y_Q(t) = -\sin[\mathbf{w}_{IF}t + \mathbf{w}_{re(n-1)}(t-t_{n-1}) + \hat{\mathbf{f}}_{re(n-1)}]y_{IF}(t) \quad \text{for } t_{n-1} \leq t < t_n \quad (24b)$$

The value $\mathbf{w}_{IF} = 2\pi \times 3.636 \times 10^6$ rad/sec is used as the nominal mixing frequency.

The next part of the simulation models the PRN code play-back NCO, the code mixers, and the integrate-and-dump accumulators. As far as the PLL is concerned, these actions effectively perform the following calculations to determine the in-phase and quadrature accumulations:

$$I_{(n)} = \frac{1}{0.001} \int_{t_{n-1}}^{t_n} y_I(t) C[\hat{\mathbf{f}}(t)] \left[\frac{d\hat{\mathbf{f}}}{dt} \right] dt \quad (25a)$$

$$Q_{(n)} = \frac{1}{0.001} \int_{t_{n-1}}^{t_n} y_Q(t) C[\hat{\mathbf{f}}(t)] \left[\frac{d\hat{\mathbf{f}}}{dt} \right] dt \quad (25b)$$

where the PRN code, $C[\hat{\mathbf{f}}]$, and the estimated code phase, $\hat{\mathbf{f}}(t)$, both correspond to the tracked GPS satellite. The actual calculations are digital summations that approximate these integrals. The summations break the integration intervals up into 10230 sub-intervals and perform Euler integration.

The simulation also emulates a DLL. This involves the calculation of early and late accumulations, similar to eqs. (25a) and (25b) but with offsets of $\hat{\mathbf{f}}$. Another part of the DLL simulation is a carrier-aided proportional feedback control law that adjusts $d\hat{\mathbf{f}}/dt$ of its PRN play-back NCO. The goal of this feedback controller is to align $\hat{\mathbf{f}}(t)$ with the actual $\mathbf{f}(t)$ of the received signal's code. The control law is

$$\begin{aligned} \hat{\mathbf{w}}_{n+1.5} &= \hat{x}_{v(n)} + (1.5 \mathbf{D}t_n) \hat{x}_{a(n)} \\ &+ \mathbf{w}_a \{-\hat{x}_{c(n)} \sin[\mathbf{w}_a(t_n + 1.5 \mathbf{D}t_n) + \mathbf{y}_{a0}]\} \end{aligned}$$

$$+ \hat{x}_{s(n)} \cos[\mathbf{w}_a(t_n + 1.5 \mathbf{D}t_n) + \mathbf{y}_{a0}] \quad (26a)$$

$$\left[\frac{d\hat{\mathbf{f}}}{dt} \right]_{n+1} = 1 + K_{DLL}(\mathbf{t} - \hat{\mathbf{f}})_n + \frac{\hat{\mathbf{w}}_{n+1.5}}{\mathbf{w}_c} \quad (26b)$$

K_{DLL} is the proportional gain. A value of $2p$ has been used for K_{DLL} , which corresponds to a 1 Hz bandwidth for the DLL. The code phase error term, $(\mathbf{t} - \hat{\mathbf{f}})_n$, is computed from the difference between early and late accumulations for the time interval t_{n-1} to t_n . This type of computation is described in Ref. 12. The last term on the right-hand side of eq. (26b) is the carrier aiding term; $\hat{\mathbf{w}}_{n+1.5}$ is a prediction of what the signal's average Doppler shift will be during the time interval from t_{n+1} to t_{n+2} .

The simulation's PLL loop filter calculations have already been described in Section IV. They are given in eqs. (8), (13a), (13b), and (16).

The effects of receiver clock errors have been incorporated using a two-state drift model from Ref. 18. The states are $d\mathbf{t}_{rc}$, the time error, and $d\mathbf{f}_{rc}$, the fractional frequency error. Their dynamic models are:

$d\mathbf{t}_{rc} = d\mathbf{f}_{rc} + w_{1rc}$ and $d\mathbf{f}_{rc} = w_{2rc}$. The white noise processes w_{1rc} and w_{2rc} drive the drift with intensities $E\{w_{1rc}(t)w_{1rc}(\mathbf{t})\} = 0.5h_0d(t-\mathbf{t})$ and $E\{w_{2rc}(t)w_{2rc}(\mathbf{t})\} = 2p^2h_2d(t-\mathbf{t})$. The constants h_0 and h_2 define the level of drift. This clock drift model impacts the rest of the simulation through eq. (8). The average value of the quantity $\mathbf{w}_c d\mathbf{t}_{rc}$ during the accumulation interval from t_{n-1} to t_n gets subtracted from the right-hand side of eq. (8). This models the effect of receiver clock drift on the PLL's measurement of the carrier phase error.

The simulation operates iteratively and must be initialized. It processes one PRN code period interval at a time, and it uses some of the outputs from the interval t_{n-1} to t_n as the inputs to the interval t_n to t_{n+1} . In order to initialize the process, the simulation needs to start with guesses of the Kalman filter state, \hat{x} , the NCO phase, $\hat{\mathbf{f}}_{rc}$, the estimated PRN code phase, $\hat{\mathbf{f}}$, the PLL's NCO rate, \mathbf{w}_{rc} , and the DLL's NCO rate, $d\hat{\mathbf{f}}/dt$. In order to achieve lock, these guesses need to be fairly accurate. Any real receiver has a start-up mode that searches to find good initial guesses for such quantities. After the search is complete, the receiver locks onto the GPS signal and tracks it for a long time. The system's acquisition-mode performance does not impact its accuracy during this steady-state period. Therefore, fairly good first guesses of the above quantities have been used, and the issue of signal acquisition has not been considered in the present study.

VI. Evaluation of Attitude Sensing Performance

The simulation and miscellaneous analyses have been used to evaluate the attitude sensing accuracy of the system. There are a number of issues that have been investigated in order to determine the system's expected performance. Thermal and digitization noise, interference from other GPS satellites, receiver clock drift, and receiver distortion all might cause attitude sensing errors. The amount by which these effects degrade accuracy needs to be investigated. Some of these errors can be reduced by reducing the attitude sensing bandwidth, and the relationship between bandwidth and accuracy must be determined. Other system parameters that may affect accuracy are turntable rotation speed, w_a , antenna mounting radius, r_a , and the elevation angle of the tracked GPS satellite above the turntable's plane of rotation, q . These parameters' effects also need to be investigated. Also at issue is whether the system can distinguish small periodic integrated Doppler shift variations that ride on top of the Doppler shifts that are caused by large line-of-sight velocities and accelerations.

An example case has been evaluated using the simulation. It is characterized by the following parameters: The antenna mounting radius is $r_a = 0.1$ m, and the turntable speed is $w_a = 419$ rad/sec (4000 RPM). The tracked GPS satellite has an elevation angle of $q = \pi/4$ rad (45 deg). The thermal/digitization noise level of the antenna and receiver combine with the level of the received signal's power to yield an SNR of 18 dB for the I_n and Q_n accumulator outputs. This SNR level corresponds to a 7.2-deg RMS phase measurement noise at the 1000 Hz sampling frequency. The clock drift parameters are those of a representative ovenized crystal oscillator: $h_0 = 2 \times 10^{-22}$ sec and $h_2 = 6.1 \times 10^{-22}$ /sec. The gain for the attitude sensing part of the Kalman filter is $L_{cs} = 0.008$, which yields a 0.64 Hz attitude sensing bandwidth. The filter gain component L_{pva} equals $[0.0426, 0.9135, 9.7869]^T$. This produces a 3.4 Hz velocity/acceleration determination bandwidth, and the characteristic values of this part of the Kalman filter form a 3-pole Butterworth pattern. The initial velocity and acceleration of the line of sight from the turntable center to the tracked GPS satellite are $\dot{\mathbf{r}}_{s0} = 6000$ m/sec and $\ddot{\mathbf{r}}_s = 50$ m/sec² (5 g's). The tracked satellite transmits PRN code number 8. There are 8 interfering GPS satellites, all with the same received power level as the tracked satellite. These interfering signals reduce the SNR at the I_n and Q_n outputs by 1 dB.

Figure 3 shows the estimation errors for q (solid line) and y_s (dash-dotted line) for this case. During the

first half second of the simulation the Kalman filter converges from initial errors. Afterwards, it settles into a steady state. Both angles have steady-state RMS errors of 0.2 deg and peak steady-state errors of about 0.6 deg. This is relatively coarse attitude accuracy.

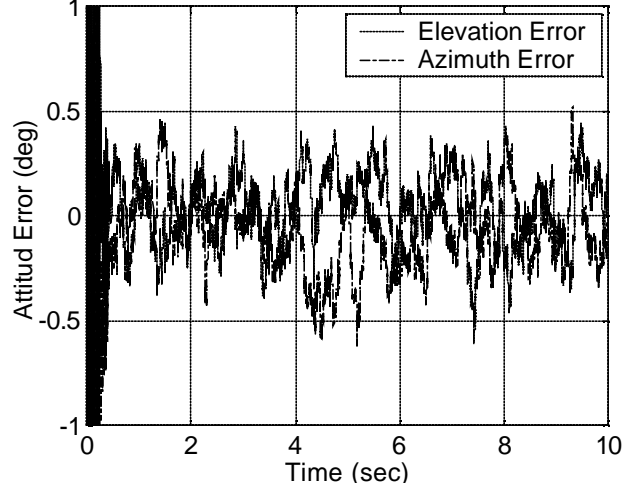


Fig. 3. Attitude estimation errors for a typical case.

In order to explore system accuracy in various situations, it is helpful to parameterize the attitude in terms of the unit direction vector to the tracked GPS spacecraft, $\hat{\mathbf{r}}_s$. One can use x_c and x_s to directly calculate this vector. Equations (4a) and (4b) and the geometry of Fig. 1 imply that

$$\hat{\mathbf{r}}_s = \begin{bmatrix} \left(\frac{c}{w_c r_a} \right) x_c \\ \left(\frac{c}{w_c r_a} \right) x_s \\ \sqrt{1 - \left(\frac{c}{w_c r_a} \right)^2 (x_c^2 + x_s^2)} \end{bmatrix} \quad (27)$$

The covariance of the $\hat{\mathbf{r}}_s$ estimation error can be calculated from the covariance of the x_c and x_s estimation errors. Suppose that these latter two quantities' estimation errors are uncorrelated and that their standard deviations both equal \mathbf{s}_{cs} . (This is a good approximation for the Kalman filter whose gain is given in eq. (14) if the turntable rotation speed is high enough.) Then the $\hat{\mathbf{r}}_s$ vector's (linearized) estimation error covariance matrix is

$$E\{[\hat{\mathbf{r}}_{s(est)} - \hat{\mathbf{r}}_{s(actual)}][\hat{\mathbf{r}}_{s(est)} - \hat{\mathbf{r}}_{s(actual)}]^T\} = \left(\frac{\mathbf{s}_{cs} c}{w_c r_a} \right)^2 \left(\hat{\mathbf{y}}_y \hat{\mathbf{y}}_y^T + \frac{1}{\sin^2 q_s} \hat{\mathbf{q}}_q \hat{\mathbf{q}}_q^T \right) \quad (28)$$

where $\hat{\mathbf{y}}_y = [-\sin y_s, \cos y_s, 0]^T$ and $\hat{\mathbf{q}}_q = [-\cos y_s \sin q_s, -\sin y_s \sin q_s, \cos q_s]^T$ are orthogonal unit vectors in the

directions of locally increasing \mathbf{y} , and \mathbf{q}_s , respectively.

Equation (28) gives the key to understanding the effects on the system's accuracy of various design parameters. The directional standard deviations for \hat{r}_s estimation errors are:

$$\mathbf{s}_{el} = \left(\frac{\mathbf{s}_{cs}c}{\mathbf{w}_c r_a} \right) \frac{1}{\sin \mathbf{q}_s} \quad (29a)$$

$$\mathbf{s}_{az} = \left(\frac{\mathbf{s}_{cs}c}{\mathbf{w}_c r_a} \right) \quad (29b)$$

where \mathbf{s}_{el} is measured in the elevation direction and \mathbf{s}_{az} is measured in the azimuthal direction. The simulations and analyses have shown that \mathbf{s}_{cs} , the standard deviation of x_c and x_s , depends only on the filter's bandwidth and the input signal-to-noise ratio for the channel. The quantities c and \mathbf{w}_c are fixed parameters. Therefore, the only ways to affect system accuracy are to change the antenna mounting radius on the turntable, r_a , the bandwidth of the filter, or the input signal-to-noise ratio of the receiver/antenna system.

Equation (29a) says that the elevation accuracy increases with increasing elevation, reaching its maximum when $\mathbf{q}_s = 90$ deg. At $\mathbf{q}_s = 0$ deg the elevation standard deviation goes to infinity. In other words, the best vector attitude sensing geometry occurs when the tracked GPS satellite is lined up on the turntable's rotation axis, and the worst geometry occurs when the tracked satellite is in the turntable plane – review Fig. 1.

There is obviously a lower bound on the useable elevation window if one wants to get a reasonable vector attitude measurement from the system. Elevations down as low as $\mathbf{q}_s = 45$ deg are certainly useable, as demonstrated by the results in Fig. 3. At 45 deg, the RMS elevation error is only 41% larger than it is at $\mathbf{q}_s = 90$ deg.

A full 3-axis attitude solution requires that the system track 2 or more non-collinear GPS satellites. Therefore, at least some of the tracked GPS satellites must have elevations significantly below 90 deg. This requirement should not present a problem. In fact, it would be acceptable to track a satellite with very low turntable-relative elevation if azimuth information was the only information which was needed from that satellite.

The simulation results have borne out this analysis. When r_a is increased, attitude errors decrease proportionately. When \mathbf{q}_s is increased, elevation errors decrease as $1/\sin \mathbf{q}_s$. The use of different turntable speeds does not affect attitude error, to a certain point, if one uses an ovenized crystal oscillator with stability characteristics like those that have been used in the Fig.-3 example. Turntable speeds as low as 105

rad/sec. (1000 RPM) have been simulated without changing any other parameters, and the system's performance has been virtually unchanged. Of course, if very low turntable speeds are used, then the attitude error will be affected, either because of excessive receiver clock drift or because of violation of the bandwidth assumption that is associated with the periodic Kalman filter gain approximation in eq. (14).

The effect of receiver clock stability has been investigated. The example that produced Fig. 3 has been re-run with a less stable receiver clock, one whose drift model is characterized by the parameters $h_0 = 2 \times 10^{-19}$ sec and $h_2 = 2 \times 10^{-20}$ /sec. This corresponds to a temperature-compensated crystal oscillator¹⁸. The attitude determination performance deteriorates significantly in this case. The RMS elevation and azimuth errors increase to 0.5 deg. Furthermore, the system sensitivity to rotor speed increases when this poorer receiver clock is used. If the wheel speed is decreased from 4,000 RPM to 1,000 RPM, then the RMS attitude errors increase to about 1.5 deg.

It should be noted at this point that there is a way to estimate and compensate for the effects of receiver clock errors. The method relies on attitude data from 3 or more GPS satellites that are in a suitable geometric relationship. The receiver-clock-induced errors in \hat{x}_c and \hat{x}_s are the same for all tracked satellites. They can be estimated by comparing the measured angles between the vectors to the tracked GPS satellites with the known values for these angles based on ephemerides. This technique is analogous to the standard receiver clock correction that is used in the GPS navigation solution. The full analysis of this technique is not given here because it is beyond the scope of this paper.

The simulation results show that performance is insensitive to several environmental and system disturbances. Interference from other GPS satellites does not significantly affect performance at practically achievable SNRs. Receiver distortion in the RF front end also has little effect. The attitude sensing accuracy does not degrade if large Doppler shifts and Doppler shift rates get induced by large velocities and accelerations of the turntable's center.

Attitude sensing accuracy can be increased by lowering the filter bandwidth or by raising the SNR. A simple calculation shows that \mathbf{s}_{cs} scales as the square root of filter bandwidth divided by signal-to-noise ratio, and the simulation results have borne this out.

Suppose that one wanted to improve the accuracy of the case associated with Fig. 3. Suppose that the accuracy goal was to reduce the RMS elevation error

to 0.03 deg. Recall that Fig. 3 shows a steady-state RMS elevation error of 0.2 deg and that the attitude sensing filter bandwidth is 0.64 Hz. The filter bandwidth would have to be reduced to 0.014 Hz in order to meet the 0.03 deg accuracy goal. Such a filter would have an effective delay of 11 sec when operating on a dynamically varying attitude signal, which would be unacceptable performance in many situations. The filter associated with Fig. 3 has a delay of only 0.25 sec. If one wanted to make the same accuracy improvement via reduction of receiver noise, then an increase of 16 dB in the SNR would be needed. Such an increase is probably not feasible.

Another way to increase accuracy is to lower the filter bandwidth while augmenting the attitude determination system with an inertial attitude measurement. One could add a tuning-fork rate gyro in order to get acceptable bandwidth with respect to real dynamic attitude variations while simultaneously lowering the bandwidth of the GPS part of the system. This type of approach has been tried successfully with a multi-antenna-based GPS attitude sensing system¹⁹, and it would probably work well with the rotating-antenna system. Such an approach would work best if the attitude determination Kalman filter were coupled to the receiver's PLL.

There may be a practical way to increase accuracy by drastically increasing the mounting radius of the antenna, r_a . There are practical limitations to the size of a physical turntable, but these limitations can be overcome if one electrically simulates an antenna on a turntable. One way to do this would be to mount a large ring of patch antennas on the user vehicle. An RF switching circuit would connect them to the receiver one at a time. The sequence of connection would follow a circular path, which would synthesize circular motion of the phase center of a single antenna. This is one of the methods described in Ref. 7 for radio direction finding. Note that it should be possible to use distorted circular patterns. Such a mounting pattern might be more easily realizable due to antenna location constraints on a real vehicle. If the mounting pattern is not exactly circular, then the receiver's PLL will have to be modified to account for the distortion.

One might protest that such a design would be a reversion to the original multi-antenna approach. On one level this is true, but such a system would retain the advantage of not needing many receiver channels. Furthermore, if the neighboring antennas were close enough to each other, then the system would not need to resolve integer ambiguities, yet it would have the advantages of a long baseline. Of course, this approach assumes that it is practical to mount many patch antennas and a number of RF switches on the user

vehicle.

It should be noted that, in some sense, this paper's new system is equivalent to the original multi-antenna GPS attitude sensing scheme. Instead of using multiple antennas, it uses one antenna at multiple locations. Although this scheme has several advantages, it retains some of the basic limitations of the multi-antenna system. The most important common limitation is that both systems' accuracies vary in the same way with bandwidth and with antenna baseline length (r_a).

This analogy allows one to make a rough estimate of the impact of multi-path errors on accuracy. Multi-path has been found to induce 0.005 m RMS differential carrier phase ranging errors between pairs of static antennas¹. It is reasonable to suppose that this differential error magnitude will hold true for the present system's single antenna if the difference is taken between times when the antenna is on opposite sides of its circular path. In this case, the attitude error will be $0.005\text{m}/(2r_a)$ radians. For $r_a = 0.1$ m this translates into an RMS attitude error of 1.4 deg. Thus, multi-path error will dominate all other error sources unless the system uses a low-stability oscillator in its receiver and a low turntable speed. Multi-path errors can be reduced by increasing, r_a , the mounting radius of the antenna.

Conclusions

A system that senses vector attitude information using a single GPS antenna has been proposed and analyzed. The antenna is mounted on a turntable with its phase center offset from the rotation axis. The resulting circular motion causes periodic phase modulation of the received GPS carrier signal. This periodic modulation can be detected by using a special loop filter in the receiver's carrier tracking phase-locked loop. The amplitude and phase of the modulation can be used to deduce the direction vector to the tracked GPS satellite in receiver vehicle coordinates. This vector measurement is an attitude measurement, and two such vector measurements are sufficient to determine the 3-axis attitude of the user vehicle.

The proposed system has been analyzed, and it has been evaluated using a time-domain simulation. A 1- σ accuracy of 1.4 deg has been demonstrated for a system that uses a 0.1 m antenna mounting radius, a 4,000 RPM turntable speed, an ovenized crystal oscillator for its receiver clock, and a 0.64 Hz phase-locked loop bandwidth. The attitude error standard deviation is inversely proportional to the antenna mounting radius. The accuracy is essentially independent of the turntable rotation speed if that

speed is significantly larger than the sensor's bandwidth and if the receiver clock is sufficiently stable. The dominant error source in the system comes from multi-path reflections.

Acknowledgments

This work was supported in part by NASA through Contract Number NAS5-32815 to Ithaco Space Systems. Seymor Kant was the NASA contract monitor, and Bruce Wolfe oversaw the contract work for Ithaco.

References

1. Cohen, C.E., "Attitude Determination," in *Global Positioning System: Theory and Applications, Vol. II*, Parkinson, B.W. and Spilker, J.J. Jr., eds., American Institute of Aeronautics and Astronautics, (Washington, 1996), pp. 519-538.
2. Psiaki, M.L., Theiler, J., Bloch, J., Ryan, S., Dill, R.W., and Warner, R.E. "ALEXIS Spacecraft Attitude Reconstruction with Thermal/Flexible Motions Due to Launch Damage", *Journal of Guidance, Control, and Dynamics*, Vol. 20, No. 5, 1997, pp. 1033-1041.
3. Bar-Itzhack, I.Y., Montgomery, P.Y., and Garrick J.C., "Algorithms for Attitude Determination Using the Global Positioning System," *Journal of Guidance, Control, and Dynamics*, Vol. 21, No. 6, 1998, pp. 846-852.
4. Kornfeld, R.P., Hansman, R.J., and Deyst, J.J., "Single Antenna GPS Based Aircraft Attitude Determination," *Proceedings of the Institute of Navigation National Technical Meeting*, Institute of Navigation, Alexandria, Virginia, 1998, pp. 345-354.
5. Martín-Neira, M. and Lucas, R., "GPS Attitude Determination of Spin Stabilized Satellites," *Proceedings of ION GPS-92*, Institute of Navigation, Alexandria, Virginia, 1992, pp. 757-765.
6. Axelrad, P. and Behre, C.P., "Attitude Estimation Algorithms for Spinning Satellites Using Global Positioning System Phase Data," *Journal of Guidance, Control, and Dynamics*, Vol. 20, No. 1, 1997, pp. 164-169.
7. Kennedy, H.D. and Woolsey, R.B., "Direction-Finding Antennas and Systems," in *Antenna Engineering Handbook, 3rd Edition*, R.C. Johnson, ed., McGraw-Hill, (New York, 1993), pp. 39-1 to 39-37.
8. Anon., *GPS Builder-2 Designer's Guide*, GEC Plessey Semiconductors, Wiltshire, U.K., April, 1995.
9. Anon., <http://www.ithaco.com/T-Scanwheel.html>, edited by Susan Golden & Associates, Ithaco Space Systems, Ithaca, N.Y., 1997.
10. Bar-Itzhack, I.Y., "REQUEST: A Recursive QUEST Algorithm for Sequential Attitude Determination," *Journal of Guidance, Control, and Dynamics*, Vol. 19, No. 5, 1996, pp. 1034-1038.
11. Axelrad, P. and Brown, R.G., "GPS Navigation Algorithms," in *Global Positioning System: Theory and Applications, Vol. I*, Parkinson, B.W. and Spilker, J.J. Jr., eds., American Institute of Aeronautics and Astronautics, (Washington, 1996), pp. 409-433.
12. Spilker, J.J. Jr., "Fundamentals of Signal Tracking Theory," in *Global Positioning System: Theory and Applications, Vol. I*, Parkinson, B.W. and Spilker, J.J. Jr., eds., American Institute of Aeronautics and Astronautics, (Washington, 1996), pp. 245-327.
13. Van Dierendonck, A.J., "GPS Receivers," in *Global Positioning System: Theory and Applications, Vol. I*, Parkinson, B.W. and Spilker, J.J. Jr., eds., American Institute of Aeronautics and Astronautics, (Washington, 1996), pp. 329-407.
14. Stengel, R.F., *Optimal Control and Estimation*, Dover, (New York, 1994), pp. 150, 361-364.
15. Psiaki, M.L., "Magnetic Torquer Attitude Control via Asymptotic Periodic Linear Quadratic Regulation," to appear in the *Journal of Guidance, Control, and Dynamics*. Currently available at http://www.mae.cornell.edu/Psiaki/magtorquer_a_lqr.pdf.
16. Couch, L.W. II, *Digital and Analog Communication Systems, 4th Ed.*, Macmillan, (New York, 1993), pp. 242-261.
17. Spilker, J.J. Jr., "GPS Signal Structure and Theoretical Performance," in *Global Positioning System: Theory and Applications, Vol. I*, Parkinson, B.W. and Spilker, J.J. Jr., eds., American Institute of Aeronautics and Astronautics, (Washington, 1996), pp. 57-119.
18. Brown, R.G. and Hwang, P.Y.C., *Introduction to Random Signals and Applied Kalman Filtering, 3rd Edition*, J. Wiley & Sons, (New York, 1997), pp. 428-432.
19. Gebre-Egziabher, D., Hayward, R.C., and Powell, J.D., "A Low-Cost GPS/Inertial Attitude Heading Reference System (AHRS) for General Aviation Applications," *Proceedings of the IEEE 1998 Position, Location, and Navigation Symposium*, April 20-23, 1998, Palm Springs, CA, pp. 518-525.